Characterizing Stiffness and In-situ Stress Anisotropies from Pressuremeter Testing

Caractérisation de la rigidité et des anisotropies de contrainte in situ à partir d'essais pressiométriques

Lang Liu[1#] , Rick Chalaturnyk[2], Derek Martin[2], Silvio Giger[3], Haifeng Fu[4]

[1]*SINTEF, Department of Applied Geoscience, Trondheim, Norway*
[#]*Corresponding author: lang.liu@sintef.no*
[2]*University of Alberta, Department of Civil & Environmental Engineering, Edmonton, Canada*
[3]*Nagra, Section of Hydrogeology & Geomechanics, Wettingen, Switzerland*
[4] *CNPC, Research Institute of Petroleum Exploration and Development, Langfang, China*

ABSTRACT

This study explored the use of pressuremeter testing (PMT) to characterize stiffness and in-situ stress anisotropies. By integrating multi-caliper deformation measurements with analytical and numerical modeling, this study demonstrated that deformation anisotropies, such as in Opalinus Clays, can be effectively resolved. Transversely isotropic elastic parameters were estimated by fitting the apparent borehole moduli derived from the PMT unloading data, whereas the anisotropic creep behavior was captured using a viscoelastic model implemented in a finite element (FE) simulation. Controlled laboratory experiments under known polyaxial stress conditions revealed that borehole expansion after yielding reflects the orientation and magnitude of the horizontal stress anisotropy. These observations were further supported by FE simulations, which enabled an inversion procedure to estimate the horizontal boundary stresses based on post-yield deformation. The findings highlight the potential of advanced pressuremeter test interpretation as a practical approach for in-situ geomechanical characterization.

RESUME

Cette étude explore l'utilisation des essais pressiométriques (PMT) pour caractériser l'anisotropie de la raideur et des contraintes in situ dans les formations géologiques profondes. En intégrant des mesures de déformation multi-directionnelles avec des modèles analytiques et numériques, les résultats montrent que les anisotropies élastiques et viscoélastiques dans les géomatériaux stratifiés, tels que les schistes, peuvent être efficacement identifiées. Les paramètres élastiques d'un matériau transverse isotrope ont été estimés en ajustant les modules apparents du forage dérivés des données de déchargement du PMT, tandis que le comportement de fluage anisotrope a été reproduit à l'aide d'un modèle viscoélastique implémenté dans une simulation par éléments finis (FE). Des expériences en laboratoire sous contraintes polyaxiales contrôlées ont montré que l'expansion du forage après le seuil de plasticité reflète l'orientation et l'intensité de l'anisotropie des contraintes horizontales. Ces observations ont été confirmées par des simulations EF, qui ont permis de mettre en œuvre une procédure d'inversion pour estimer les contraintes horizontales à partir de la déformation post-plastique. Ces résultats mettent en évidence le potentiel de l'interprétation avancée des essais PMT comme approche pratique pour la caractérisation des contraintes in situ en milieux profonds.

Keywords: Pressuremeter testing; Rock anisotropy; In-situ stress anisotropy; Interpretation.

1. Introduction

Pressuremeter testing has long been recognized as an effective in-situ method for determining geotechnical parameters in shallow ground conditions (Mair and Muir Wood 1987; Clarke 2023). With advancements in pressure capacity and displacement measurement resolution, pressuremeter testing has been increasingly applied to deep rock formations (Liu et al. 2021; Hughes, and Whittle 2022). Modern pressuremeter probes are equipped with internal calipers capable of detecting borehole deformation with sub-micron precision, reaching resolutions as fine as approximately 0.1 μm. Moreover, the inclusion of multiple caliper sets oriented along different diametric axes enables the detection of anisotropic borehole deformation during testing (Figure 1).

The concept of measuring radial displacement along multiple axes in pressuremeter or dilatometer testing was introduced in earlier studies (Rocha 1970; Zalesky et al. 2007). However, these studies provide a limited interpretation of rock or rock mass anisotropy based on the collected data. Efforts to interpret in-situ stress anisotropy within the borehole cross-sectional plane were also made using self-boring pressuremeter tests in shallow ground (Dalton and Hawkins 1982). They proposed that anisotropic in-situ stress could be inferred

from the non-uniform lift-off pressures recorded by different calipers. However, this approach was later challenged by Mayu (1987), who demonstrated that the interpretation was highly sensitive to probe orientation and installation conditions.

In this paper, we present recent findings on the use of multi-caliper pressuremeter testing to characterize both stiffness anisotropy in rock and in-situ stress anisotropy. The results offer new insights into the interpretation of anisotropic ground behavior in deep formations.

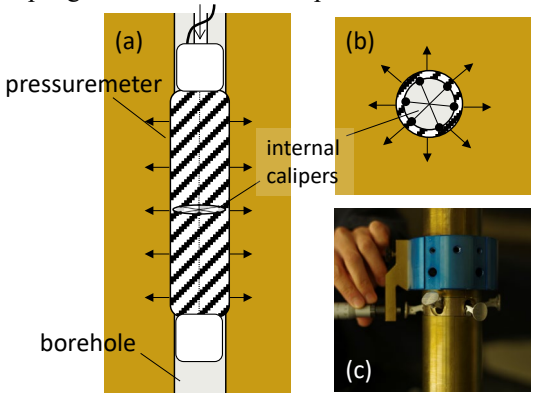

Figure 1. Schematics of pressuremeter testing in (a) borehole side and (b) cross-section views; (c) high-resolution internal calipers under laboratory calibration.

2. Influence and Interpretation of Rock Anisotropy

In a recent field campaign at the Mont Terri Rock Laboratory, a series of pressuremeter tests were conducted in three boreholes to characterize the in-situ elastic stiffness of Opalinus Clay (Liu et al. 2022). At the test site, the Opalinus Clay exhibits a bedding dip angle of approximately 40°. Among the tested boreholes, borehole BGC-A4 was oriented perpendicular to the bedding planes, whereas borehole BGC-A6 was drilled horizontally, parallel to the bedding.

Representative test results from these two boreholes—referred to as Test I (BGC-A4) and Test II (BGC-A6)—are presented in Figure 2. The figure shows the radial deformation measured using calipers along three orthogonal axes. Deformation is expressed as the normalized radial displacement u_r/r_0, where u_r is the measured radial displacement, and r_0 is the initial borehole radius.

In Test I, the deformation responses recorded along the three axes were generally consistent, except during the initial nonlinear loading phase, which may reflect the effects of nonuniform borehole disturbance. In contrast, Test II exhibited more pronounced variations in deformation across the axes. This axis-dependent response indicates the influence of inherent rock anisotropy, as borehole compliance varies with orientation relative to bedding.

Each test incorporated multiple pressure levels, during which a pressure hold of approximately five minutes was applied, followed by an unload–reload cycle with a small stress amplitude (Figure 3). The pressure-hold data were used to assess the time-dependent (creep) deformation of the borehole, whereas the unloading data provided estimates of the elastic moduli corresponding to the local borehole response.

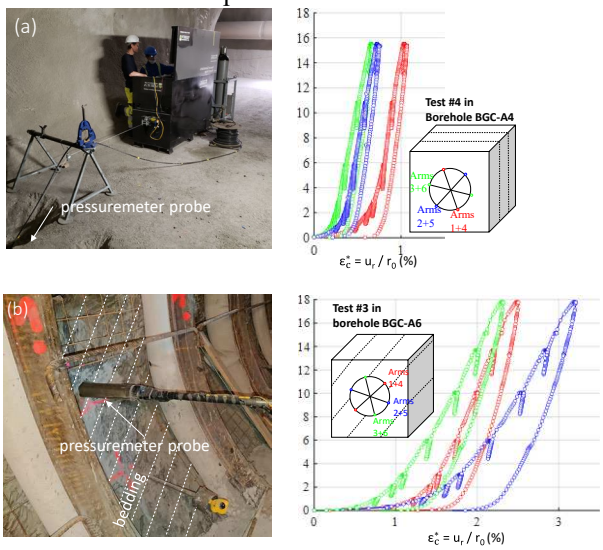

Figure 2. Pressuremeter tests in (a) an inclined borehole drilled perpendicular to bedding and (b) a horizontal borehole drilled parallel to bedding at Mont Terri Rock Laboratory with demonstration test data.

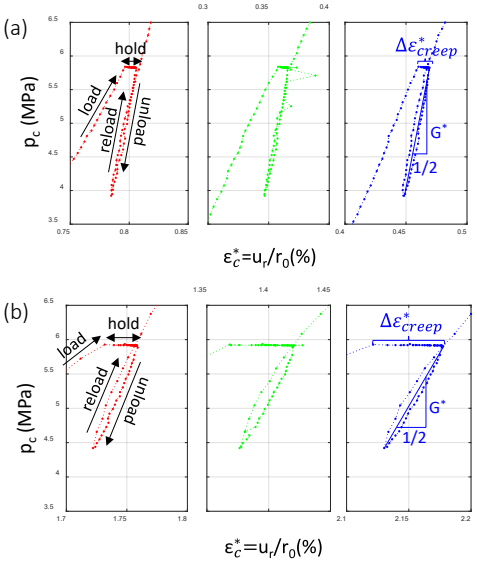

Figure 3. Zoom-in view of the data at the pressure-hold stage followed by an unload-reload cycle from (a) Test I and (b) Test II.

2.1.1. Anisotropic Elastic Response

In the two previously described tests, the data obtained from the unloading steps can be used to determine the elastic properties, assuming that the viscous effects are negligible during unloading. A convenient metric for evaluating anisotropy in the elastic borehole response is the *apparent borehole modulus*, denoted as

$$G^* = \frac{\Delta p_c}{2\Delta\varepsilon_c^*} = \frac{\Delta p_c r_0}{2\Delta u_r} \quad (1)$$

The variations in G^* measured along the three orthogonal caliper axes are shown in Figure 4. In Test I, the values of G^* were nearly identical across all axes, confirming isotropic elastic behavior within the bedding plane. In contrast, Test II revealed significant directional dependence in G^* with the maximum value aligned

approximately parallel to the bedding, indicating anisotropy.

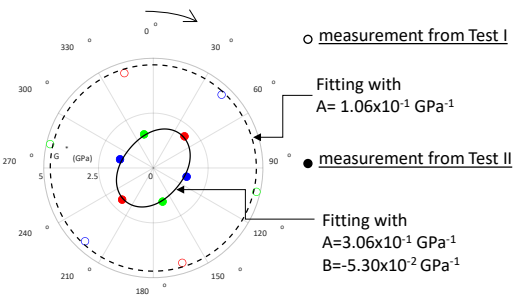

Figure 4. Apparent borehole modulus G^* determined using unloading steps from two cases of tests versus fits using analytical solution; bedding dips at $\theta = 40^o$

According to the closed-form solution derived by (Amadei and Savage 1991), G^* for a transversely isotropic material can be expressed as a function of azimuth θ,

$$G^*(\theta) = A + B\,cos(2\theta) + C\,sin(2\theta) \tag{2}$$

where the coefficients A, B, and C depend on the five independent elastic constants of a transversely isotropic medium: E_h - Young's modulus in the bedding plane, E_v - Young's modulus perpendicular to bedding, ν_{hh} - in-plane Poisson's ratio, ν_{vh} - cross-plane Poisson's ratio, and G_{vh} - shear modulus in the bedding-normal plane. Particularly, for the case where pressuremeter loading is parallel to bedding (Test I), B and C vanish, and

$$A = \frac{(1+\nu_{hh})}{E_h} \tag{3}$$

For the case where the borehole is parallel to bedding (Test II), C vanishes, and A and B have the following expressions,

$$A = \frac{1}{2}\left(\sqrt{\frac{-2C_2 + \left(C_1 + \sqrt{C_1 C_3}\right)\times}{\frac{2C_2 + C_4}{C_1} + 2\sqrt{\frac{C_3}{C_1}} - 2\sqrt{C_1 C_3}}}\right)$$
$$B = \frac{1}{2}\left(\left(C_1 - \sqrt{C_1 C_3}\right)\sqrt{\frac{2C_2 + C_4}{C_1} + 2\sqrt{\frac{C_3}{C_1}}}\right) \tag{4}$$

where $C_1 = \frac{1}{E_h}(1 - \upsilon_{hh}{}^2), C_2 = \frac{-\upsilon_{vh}}{E_v}(1+\upsilon_{hh}), C_3 = \frac{1}{E_v}\left(1 - \frac{E_h \upsilon_{vh}^2}{E_v}\right)$, and $C_4 = \frac{1}{G_{vh}}$.

For Test I, the measured values of G^* at the three caliper axes can be fitted using Eqn. (2) with A from Eqn. (3). For Test II, both A and B in Eqn. (4) are required to capture the anisotropic response.

The transversely isotropic elastic parameters, that is, E_h, E_v, ν_{hh}, ν_{vh}, and G_{vh}, can be derived using the relationships in Eqns. (3) and (4) once the fit parameters A (and also B for Case 2) are determined. However, unique solutions for these five elastic parameters cannot be found with three relationships. In this work, as a simple demonstration, Undrained Poisson's ratios ν_{hh} and ν_{vh} are assumed with values of 0.19 and 0.42 as typical for the Opalinus Clay (Liu et al. 2024), and this allows the three moduli to be determined: E_h = 11.2 GPa, E_v = 5.0 GPa, and G_{vh} = 1.1 GPa. These results reflect the anisotropic nature of Opalinus Clay and illustrate how multi-axis pressuremeter measurements can be used to resolve directional elastic behavior.

2.1.2. Anisotropic Creep Response

The creep deformation of shales can be described using viscoelastic models (Sone and Zoback, 2013; Trzeciak et al. 2018). These models represent time-dependent stiffness relaxation under an imposed strain and are effectively captured using a finite sum of decaying exponentials, commonly referred to as a *Prony series* (Gutierrez-Lemini 2014). In three dimensions, the relaxation of the elastic stiffness tensor $\mathbf{C}(t)$ can be expressed as:

$$\mathbf{C}(t) = \mathbf{C_0}\left(1 - \sum_{i=1}^{N} k_i\left(1 - e^{-t/\tau_i}\right)\right) \tag{5}$$

where $\mathbf{C_0}$ is the reference elastic stiffness tensor at time t=0. k_i and τ_i are the modulus reduction factor and retardation time, respectively, for the ith Prony series component. For a transversely isotropic material, the compliance matrix $\mathbf{C}^{-1}$ can be expressed using the elastic parameters:

$$[\mathbf{C}]^{-1} = \begin{bmatrix} 1/E_h & -\nu_{hh}/E_h & -\nu_{vh}/E_v & 0 & 0 & 0 \\ -\nu_{hh}/E_h & 1/E_h & \nu_{vh}/E_v & 0 & 0 & 0 \\ -\nu_{hv}/E_h & -\nu_{hv}/E_h & 1/E_v & 0 & 0 & 0 \\ 0 & 0 & 0 & 1/G_{vh} & 0 & 0 \\ 0 & 0 & 0 & 0 & 1/G_{vh} & 0 \\ 0 & 0 & 0 & 0 & 0 & 1/G_{hh} \end{bmatrix} \tag{6}$$

Due to the lack of an analytical solution for cavity expansion in anisotropic viscoelastic media, a numerical approach was adopted. The above constitutive model was implemented incrementally as a UMAT subroutine in the finite element (FE) software Abaqus. A plane-strain cavity model with mesh discretization (Figure 5) was used to simulate the pressuremeter testing in a borehole oriented parallel to the bedding.

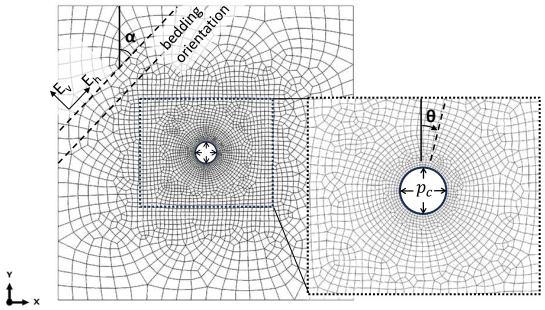

Figure 5. Finite element model of borehole oriented parallel to the plane of transverse isotropy

In the FE model, an internal pressure p_c was applied instantaneously to the borehole wall, followed by a hold period of constant pressure. The resulting radial displacement at the borehole surface over time was used to simulate viscoelastic deformation. The measured creep data from the pressure-hold step (Figure 3) were employed to calibrate the stiffness relaxation parameters k_i and τ_i in Eqn. (5).

For simplicity, only the first component of the Prony series (i.e., N=1) was considered. The elastic stiffness tensor $\mathbf{C}_0$ was fixed using values derived in the previous section. The fitting process aimed to match the model predictions with radial creep deformation measured at the three caliper axes.

The creep strain measured in Test I, where the borehole was oriented perpendicular to the bedding, showed minimal variation across the caliper axis (Figure 6), confirming isotropic viscoelastic behavior within the bedding plane. As no directional dependency was observed, the model fitting was straightforward. A good match with the FE model was obtained using the parameter values $k_1 = 0.1$ and $\tau_1 = 200$s.

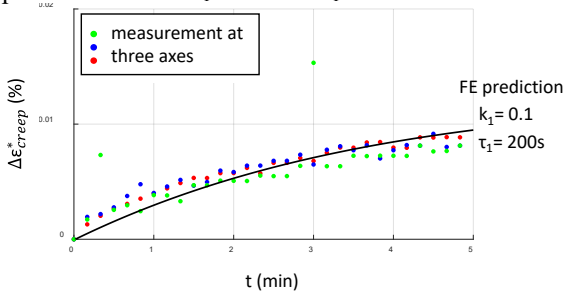

Figure 6. Creep strains measured at three caliper axes versus the predicted isotropic creep from the FE model for Test I

In Test II**,** the creep deformation varied significantly across the three axes (Figure 7), indicating an anisotropic viscoelastic response**.** When the same parameters as those used in Test I were used, the model under-predicted the observed strain magnitudes. Improved agreement was achieved by increasing the stiffness reduction factor and decreasing the retardation time to $k_1 = 0.4$ and $\tau_1 = 100$s.

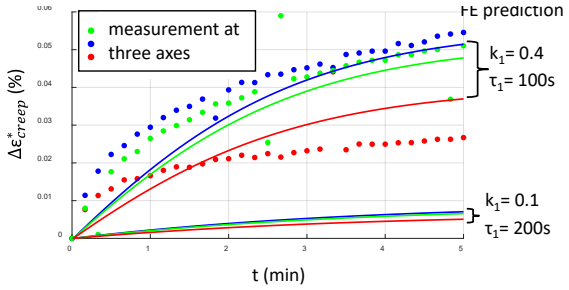

Figure 7. Creep strains measured at three caliper axes versus the predicted anisotropic creep from the FE model for Test II

The variation in creep strain $\Delta\varepsilon_c^*$ accumulated over the 5-minute hold period is presented in Figure 8. In Test II, the axis of minimum creep deformation was aligned approximately parallel to bedding, which was consistent with the predicted direction of maximum stiffness. Although the finite element model captured the orientation of the anisotropic response reasonably well, some discrepancies remained in the magnitude of the predicted deformation, indicating that further model refinement is required.

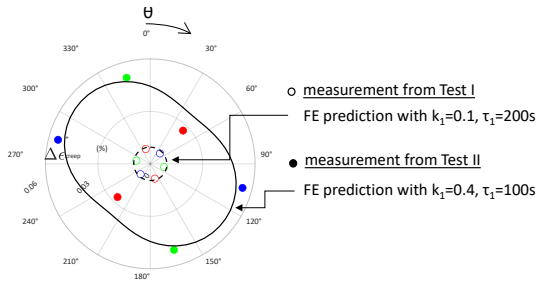

Figure 8. Circumferential variations of borehole creep after 5-minute pressure holds for two test cases versus the prediction using the FE model; bedding dips at $\theta = 40°$ in Test II.

3. Influence and Interpretation of In-situ Stress Anisotropy

An experimental study was conducted by Liu et al. (2018) to investigate the influence of anisotropic in-situ stress fields on pressuremeter testing using a polyaxial loading facility. To simulate realistic subsurface stress conditions, a large analog specimen was created by mixing Portland cement, kaolinite, and water. The resulting composite material had a Young's modulus of approximately 2 GPa and uniaxial compressive strength of approximately 10 MPa.

A cylindrical borehole was pre-drilled at the center of each cubic specimen. Prior to testing, the specimen was subjected to controlled polyaxial boundary stresses: vertical (σ_V), major horizontal (σ_H), and minor horizontal (σ_h) (Figure 9).

To assess the effects of stress anisotropy on borehole deformation, three distinct boundary stress configurations were applied to the three specimens (Table 1). In each test, a pressure-hold phase was followed by an unload–reload cycle and a final unloading phase. Radial deformations were recorded independently along three orthogonal caliper axes during the pressuremeter tests.

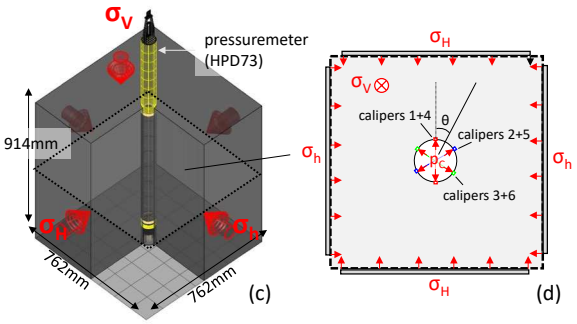

Figure 9. Schematic diagram of the experiment reported by Liu et al. (2018)

Table 1. Loading applied at the cement block boundaries in three tests

Test	σ_V(MPa)	σ_H (MPa)	σ_h (MPa)	σ_H/σ_h
#1	3	3.7	3.3	1.12
#2	2.6	3.25	2.15	1.51
#3	5	3.3	1.7	1.94

The test responses from the three caliper axes for each specimen are presented in Figure 10. Across all tests, a consistent pattern emerged in three stages: 1) Initial stage with nonlinear expansion (< 2 MPa): likely reflects borehole disturbance effects or preloading of microstructures. 2) Linear expansion stage: This stage represents the elastic deformation response of the cement matrix. 3) Nonlinear expansion stage at a high expansion pressure: indicates the onset of plastic deformation in the surrounding material. The degree of anisotropy in the radial expansion, especially at the high-pressure stage, shows the difference in deformation measured at the three caliper axes and suggests an influence of the boundary stress state on the mechanical response observed during pressuremeter testing.

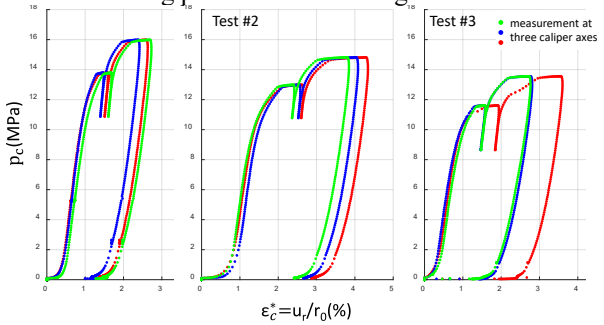

Figure 10. Test curves obtained from the three tests

3.1.1. Yield Pressure

To explain the differences in the borehole response at high expansion pressures, the evolution of the borehole stress field can be analyzed using elastic theory**.** For a plane-strain model with an isotropic elastic medium, the circumferential stress at the borehole wall is given by the classical Kirsch solution (Kirsch 1898)

$$\sigma_\theta = \sigma_H + \sigma_h - 2(\sigma_H - \sigma_h)\cos 2\theta - p_c \qquad (7)$$

The deviator stress at the borehole wall is expressed as

$$q_{ps} = \frac{1}{2}|\sigma_r - \sigma_\theta| = \left|p_c - \frac{(\sigma_H + \sigma_h)}{2} + (\sigma_H - \sigma_h)\cos 2\theta\right| \qquad (8)$$

The absolute value is used because the sign of $\sigma_r - \sigma_\theta$ depends on the relative magnitudes of the horizontal boundary stresses and the borehole pressure p_c. At the initial state, prior to borehole drilling, the deviatoric stress is $q_{ps} = (\sigma_H - \sigma_h)/2$. After drilling, $\sigma_r = 0$, and σ_θ becomes the dominant stress component at the wall. Consequently, the maximum and minimum deviator stress magnitudes were reached at $(3\sigma_H - \sigma_h)/2$ at θ = 90° and $(3\sigma_h - \sigma_H)/2$ at θ = 0°. As the pressuremeter loading increases, the uniform pressure p_c first reduces q_{ps} to zero (i.e., $\sigma_r = \sigma_\theta$) and then causes it to rise again until it reaches the material yield strength, q_y. The onset of yielding at the borehole wall occurs when $q_{ps} = q_y$. Assuming a homogeneous strength around the borehole, the expansion pressure, $p_{c,y}$, required to initiate yielding at a given azimuth θ, can be derived from Eqn. (8),

$$p_{c,y} = \frac{(\sigma_H + \sigma_h)}{2} + (\sigma_H - \sigma_h)\cos 2\theta + q_y \qquad (9)$$

Thus, yielding initiates at different pressures, depending on the borehole azimuth. For instance, $p_{c,y} = (3\sigma_h - \sigma_H)/2 + q_y$ at θ = 0° and $(3\sigma_H - \sigma_h)/2 + q_y$ at θ = 90°.

Models incorporating plasticity are used to better simulate the nonlinear expansion behavior. Zhou et al. (2016) developed a semi-analytical solution for cavity expansion under biaxial in-situ stress, assuming an elastic–perfectly plastic medium. Later studies introduced more advanced constitutive models, including the Cam-Clay model (Gong et al. 2021) and SANICLAY model (Hou et al. 2023).

In this study, a plane-strain finite element (FE) model was developed to simulate borehole expansion (Figure 11). To reduce the computational cost, only a quarter of the horizontal plane domain was modeled using symmetry conditions. The medium is assumed to obey the Tresca yield criterion with associated flow, requiring only a single parameter for plastic prediction—the yield shear strength q_y,

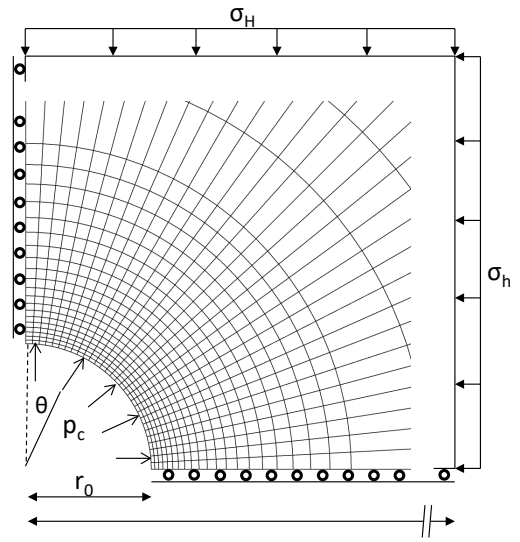

Figure 11. 2D plane-strain FE model to predict borehole expansion under anisotropic boundary stresses

The model was used to simulate Test #2, with the test data adjusted to remove deformation from the pressure–hold and unload–reload cycles (which the simplified constitutive model cannot accurately represent). Using a yield strength q_y of 3.4 MPa and shear modulus of 1067 MPa, the model captures a linear elastic expansion followed by divergent nonlinear responses depending on the azimuth after yielding (Figure 12). The predicted variation in expansion closely matched the differences observed at the three caliper axes during the test.

To identify the yield pressure more objectively, the derivative of the pressure with respect to the strain was computed for both the model and test data. In the model predictions, the onset of yielding was marked by a clear change in slope. However, in the test data, this transition is less distinct because of noise and other uncertainties.

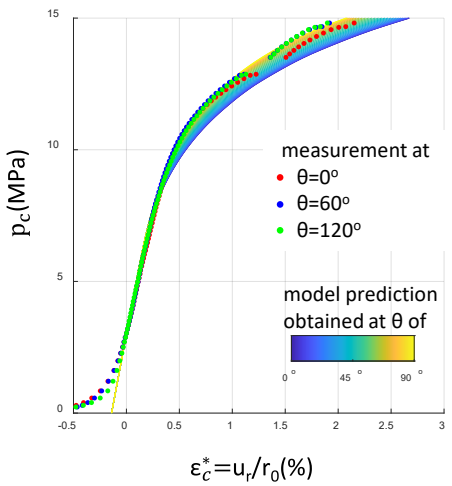

Figure 12. Model prediction of the borehole expansion at varying azimuths against the measurements from Test #2. Note that only the expansion part (without pressure-hold and unload-reload cycles) is shown in the test data.

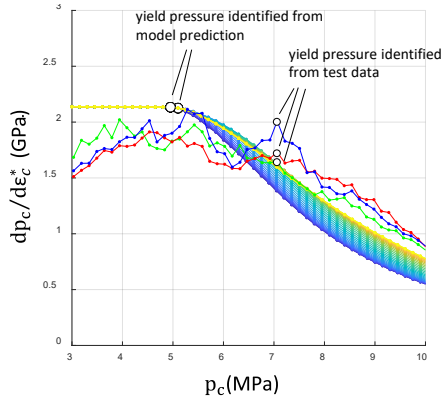

Figure 13. Identification of the yield pressures from the model prediction and test data

Finally, the yield pressures identified at different azimuths are plotted in Figure 14. Contrary to the expected azimuthal variation predicted by Eqn. (9), the results from both the experiment and prediction show little to no directional dependence. This suggests that localized yielding at any azimuth may induce nonlinear deformation at other azimuths. Consequently, yield pressures inferred from field measurements may not correspond to the actual onset of localized yielding.

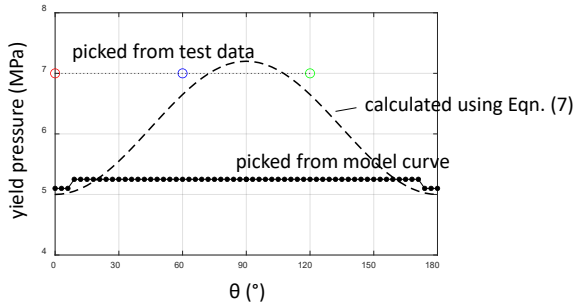

Figure 14. Model prediction of the borehole expansion at varying azimuths against the measurement from Test #2

3.1.2. Post-yield Expansion

Although yield pressures identified directly from the data remain ambiguous to use, the post-yield borehole expansion predicted by the FE model exhibited a reasonable distinction across azimuths, agreeing with the measured data. To quantify this response, the maximum borehole expansions after yielding were extracted for all three tests conducted under varying boundary stress anisotropies (Figure 15). In addition to values measured at the three caliper axes, expansions at intermediate azimuths were estimated using the interpolation method proposed by Liu et al. (2021).

Despite variations in the material strength and maximum loading pressure among the three tests, a consistent pattern was observed, wherein the maximum plastic expansion occurred near $\theta = 0^{\circ}$, which corresponds to the orientation of the major horizontal stress σ_H. Furthermore, the degree of azimuthal variation in post-yield deformation increased with the horizontal stress anisotropy ratio.

To further evaluate this behavior, FE model predictions of post-yield borehole expansion were generated for each test using the corresponding boundary stress conditions. The modeled expansions, excluding any contribution from creep, showed a reasonable alignment with the measurements. However, in Test #3, the model under-predicted the expansion near $\theta = 0^{\circ}$, where the highest deformation was recorded. This discrepancy is attributed to fracture initiation and discontinuous behavior observed during the test, which are not captured by the currently used model.

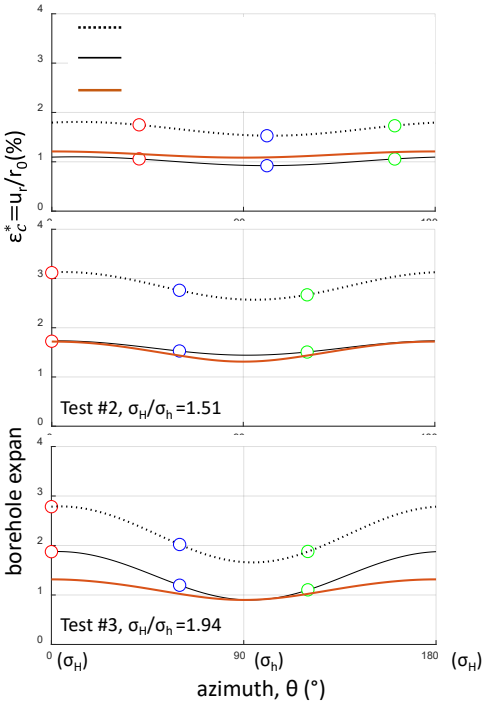

Figure 15. Variation of borehole expansion after yielding with the borehole azimuth for three tests

3.1.3. Inversion of Horizontal Stress

The overall agreement between model predictions and test data, particularly under moderate horizontal stress anisotropy, supports the use of post-yield deformation for estimating in-situ stress anisotropy. This motivates an inversion procedure, where the two horizontal boundary stresses, σ_H and σ_h, are treated as unknowns, and are iteratively adjusted in the model to

minimize the misfit between the model prediction and measurement at the caliper axes. In this case, the misfit is computed as the normalized difference between the modeled and measured strains along the loading (and unloading) histories.

Although any general-purpose optimization algorithm could be employed, the nontrivial computational cost of the FE simulations necessitates an algorithm with fast convergence and robust accuracy. Gradient-free methods, such as the Simplex approach (Nelder and Mead 1965), may be suitable. An example of the inversion to obtain the best model fit for Test #2 is presented in Figure 16. To better constrain the solution, the unloading segment of the test data was also included in the fit. The inversion begins with randomly sampled values for σ_H and σ_h within a reasonable prior range. After 71 iterations, the inversion converged to σ_H = 2.86MPa and σ_h = 2.17MPa, with 12% and 1% deviations from the true values, respectively.

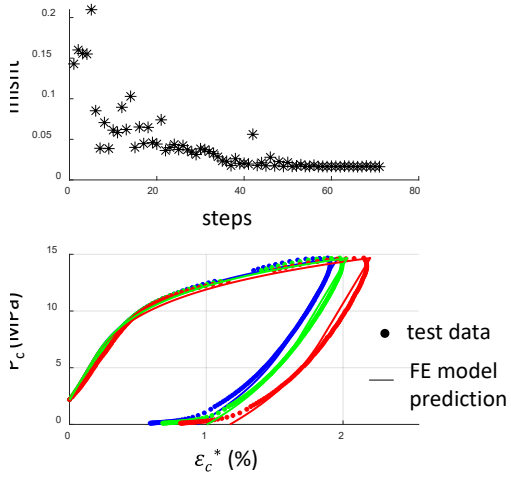

Figure 16. Finding the best model fit of Test #2 at three caliper axes through an inversion procedure. (a) the history of the misfit minimization, and (b) the best fit obtained through inversion. Note that the data from pressure hold and unload-reload cycles are excluded from the test data.

Although these results are encouraging, they do not imply guaranteed accuracy of the inverted stress values. The use of a simplified elastic–perfectly plastic constitutive model, combined with uncertainties in key material properties, such as yield strength and shear modulus, can significantly affect the inversion outcome. These uncertainties may degrade the sensitivity of the model fit to the actual boundary stresses, even when the overall misfit is small.

Therefore, it is crucial not to rely solely on the quality of the fit when interpreting stresses from pressuremeter data in practice. Reliable interpretation requires a well-calibrated understanding of the constitutive behavior of the material, consideration of parameter uncertainties in the inversion process, and cross-validation with independent measurements or prior geological knowledge, where possible.

4. Summary and Conclusions

This study investigated the potential of pressuremeter testing to characterize stiffness anisotropy and in-situ stress anisotropy in deep ground conditions using field data and controlled laboratory experiments supported by modeling. Through the integration of multi-axis caliper measurements, elastic and viscoelastic theory, and finite element simulations, several key findings were obtained.

1) Measurements with multiple calipers enable the direct observation of azimuthal variations in borehole deformation. Tests conducted in the Opalinus Clay at the Mont Terri Rock Laboratory showed clear distinctions between boreholes aligned parallel and perpendicular to bedding, confirming the sensitivity of PMT to both elastic stiffness anisotropy and viscoelastic creep anisotropy.

2) The direction-dependent mechanical behavior of the surrounding material was characterized by analyzing both the elastic and time-dependent responses. The apparent borehole moduli derived from the unloading curves were fitted using an analytical solution for transversely isotropic elasticity, enabling the estimation of directionally varying Young's and shear moduli. Additionally, borehole creep during pressure-hold sequences was modeled using a viscoelastic Prony series implemented in a finite element framework, which captured the anisotropic stiffness relaxation aligned with the bedding.

3) Laboratory-scale pressuremeter tests conducted under controlled polyaxial boundary stresses revealed that borehole deformation after yielding was strongly influenced by stress anisotropy, with maximum expansion aligning consistently with the major horizontal stress direction. These observations were supported by finite element simulations using an elastic–perfectly plastic model, which successfully reproduced the directional deformation trends. Building on this, an inversion procedure was developed to estimate the horizontal stresses (σ_H and σ_h) by minimizing the misfit between model predictions and multi-axis measurements.

This work demonstrates that advanced interpretation of pressuremeter testing, particularly when supported by multi-axis measurements and numerical modeling, can offer valuable insights into the directional mechanical behavior of geomaterials and the state of in-situ stresses. Although promising, these approaches require careful consideration of model assumptions, material variability, and inversion uncertainties. With continued development, pressuremeter-based characterization methods may significantly enhance our ability to assess stress conditions in underground environments, with broad implications for geotechnical engineering, tunneling, and deep-energy systems.

Acknowledgment

This research was primarily conducted with the support of the Reservoir Geomechanical Research Group at the University of Alberta, Canada. The authors gratefully acknowledge the technical contributions of the team members and the financial support provided by NSERC, Energi Simulation and other academic and industry research funding programs. The authors also extend their sincere appreciation to their colleagues at Nagra and Swisstopo for their assistance during the field tests at the Mont Terri Rock Laboratory and to CNPC for

their support in conducting the experiments at the polyaxial loading facility.

References

Amadei, B., and W. Z. Savage. 1991. 'Analysis of Borehole Expansion and Gallery Tests in Anisotropic Rock Masses'. *International Journal of Rock Mechanics and Mining Sciences And* 28 (5): 383–96. https://doi.org/10.1016/0148-9062(91)90077-Y.

Clarke, Barry G. 2023. *Pressuremeters in Geotechnical Design*. Second edition. Boca Raton London New York: CRC Press.

Dalton, J C P, and A B Hawkins. 1982. 'Fields of Stress - Some Measurements of the in-Situ Stress in a Meadow in the Cambridgeshire Countryside'. *International Journal of Rock Mechanics and Mining Sciences & Geomechanics Abstracts* 19 (6): 150. https://doi.org/10.1016/0148-9062(82)91606-0.

Gong, Weibing, Changyi Yang, Jingpei Li, and Lichao Xu. 2021. 'Undrained Cylindrical Cavity Expansion in Modified Cam-Clay Soil: A Semi-Analytical Solution Considering Biaxial in-Situ Stresses'. *Computers and Geotechnics* 130 (February):103888. https://doi.org/10.1016/j.compgeo.2020.103888.

Gutierrez-Lemini, Danton. 2014. *Engineering Viscoelasticity*. New York: Springer.

Hou, Lele, Xiaolin Weng, Jibo Hu, and Rongming Zhou. 2023. 'Undrained Semi-Analytical Solution for Cylindrical Cavity Expansion in Anisotropic Soils under Biaxial Stress Conditions'. *Journal of Rock Mechanics and Geotechnical Engineering* 15 (5): 1284–97. https://doi.org/10.1016/j.jrmge.2022.07.005.

Hughes, John, and Robert Whittle. 2022. *High Resolution Pressuremeters and Geotechnical Engineering*. CRC Press LLC.

Kirsch, Gustav. 1898. 'Die Theorie Der Elastizität Und Die Bedürfnisse Der Festigkeitslehre'. *Veit Ver Deut Ing* 42:797–807.

Liu, Lang, Rick Chalaturnyk, Nathan Deisman, and Gonzalo Zambrano-Narvaez. 2021. 'Anisotropic Borehole Response from Pressuremeter Testing in Deep Clay Shale Formations'. *Canadian Geotechnical Journal* 58 (8): 1159–79. https://doi.org/10.1139/cgj-2019-0801.

Liu, Lang, Haifeng Fu, Rick Chalaturnyk, and Dingwei Weng. 2018. *An Experimental Study of Pressuremeter Testing under Polyaxial Boundary Stress Sondition*. *Proceedings of GeoShanghai 2018 International Conference: Multi-Physics Processes in Soil Mechanics and Advances in Geotechnical Testing*. Vol. 1. Springer Singapore. https://doi.org/10.1007/978-981-13-0095-0.

Liu, Lang, Silvio B. Giger, Derek Martin, Rick Chalaturnyk, Kristof Schuster, Nathan Deisman, and Lukas Keller. 2022. 'In-Situ Shear Modulus Determination by Pressuremeter Tests in Opalinus Clay and Reconciliation with Laboratory Tests'. *Rock Mechanics and Rock Engineering*.

Liu, Lang, Derek Martin, Silvio B. Giger, and Rick Chalaturnyk. 2024. 'Assessment of Anisotropic Elastic Parameters Using Laboratory Triaxial and In-Situ Pressuremeter Tests in Opalinus Clay'. *Rock Mechanics and Rock Engineering*, June. https://doi.org/10.1007/s00603-024-04030-1.

Mair, R. J., and David Muir Wood. 1987. *Pressuremeter Testing: Methods and Interpretation*. CIRIA Ground Engineering Report. London : London ; Boston: CIRIA ; Butterworths.

Mayu, Philippe. 1987. 'Determining Parameters for Stiff Clays and Residual Soils Using the Self-Boring Pressuremeter'. PhD Thesis, Virginia Polytechnic Institute and State University.

Nelder, J. A., and R. Mead. 1965. 'A Simplex Method for Function Minimization'. *The Computer Journal* 7 (4): 308–13. https://doi.org/10.1093/comjnl/7.4.308.

Rocha, M. 1970. 'New Techniques in Deformability Testing of In Situ Rock Masses'. In *Determination of the In Situ Modulus of Deformation of Rock*, edited by Committee D-18, STP477-EB:0. ASTM International. https://doi.org/10.1520/STP29139S.

Sone, Hiroki, and Mark D. Zoback. 2013. 'Mechanical Properties of Shale-Gas Reservoir Rocks — Part 2: Ductile Creep, Brittle Strength, and Their Relation to the Elastic Modulus'. *GEOPHYSICS* 78 (5): D393–402. https://doi.org/10.1190/geo2013-0051.1.

Trzeciak, Maciej, Hiroki Sone, and Marcin Dabrowski. 2018. 'Long-Term Creep Tests and Viscoelastic Constitutive Modeling of Lower Paleozoic Shales from the Baltic Basin, N Poland'. *International Journal of Rock Mechanics and Mining Sciences* 112 (December):139–57. https://doi.org/10.1016/j.ijrmms.2018.10.013.

Zalesky, M, Ch B√ºhler, U Burger, and M John. 2007. 'Dilatometer Tests in Deep Boreholes in Investigation for Brenner Base Tunnel'. In *Underground Space – The 4th Dimension of Metropolises*, edited by Ivan Hrdina. Taylor & Francis. https://doi.org/10.1201/NOE0415408073.ch47.

Zhou, H., G. Kong, H. Liu, and S. L. Chen. 2016. 'A Semi-Analytical Solution for Cylindrical Cavity Expansion in Elastic–Perfectly Plastic Soil under Biaxial in Situ Stress Field'. *Géotechnique* 66 (9): 786–88. https://doi.org/10.1680/jgeot.16.P.077r.